Supporting Information for

Exploiting Multivalency and Cooperativity of Gold Nanoparticles for Binding Phosphatidylinositol (3,4,5)-trisphosphate at sub Nanomolar Concentrations

by

Flavio della Sala, Elisa Ceresara, Fabrizio Micheli, Stefano Fontana, Leonard J. Prins, Paolo Scrimin

Table of contents

1. Instrumentation and general experimental procedures

Solvents were purified by standard methods. All commercially available reagents were used as received.

$Zn(NO_3)_2$ was an analytical grade product. Metal ion stock solutions were previously titrated against EDTA following standard procedures.

Fluorescent probe **dATP_MANT** was obtained from BIOLOG Life Science Institute (Bremen, Germany) and used as received.

D-*myo*-inositol-1,4,5-triphosphate (**IP3**) and 1-stearoyl-2-arachidonoyl-*sn*-glycero-3-phospho-(1'-*myo*-inositol-3',4',5'-trisphosphate) (**PIP3**) were purchased from Avanti Polar Lipids, Inc. (Alabaster, Alabama) and used as received.

Simulated lung fluids SLF1, SLF3, the DPPC solution (1.362 mM) and **PIP3** were kindly provided by Aptuit S.r.l. (Verona, Italy). The SLF1 and SLF3 solutions and the DPPC solution were used as received, see Section 6 for composition details.

TLC analyses were performed using Merck 60 F254 pre-coated silica gel glass plates. Column chromatography was carried out on Macherey-Nagel silica gel 60 (70–230 mesh).

Milli-Q® water was obtained with a Milli-Q® EQ 7000 lab water purification system by Millipore and had resistivity of 18.2 MΩ × cm at 25 °C.

^1H NMR, ^{13}C NMR (proton decoupled) and ^{31}P NMR spectra were recorded on a Bruker AV500 operating at 500 MHz for ^1H, at 126 MHz for ^{13}C and at 202 MHz for ^{31}P.

ESI-MS measurements were acquired on an Agilent Technologies 1100 Series LC/MSD Trap-SL spectrometer, equipped with an ESI source, hexapole filter and ionic trap.

Zeta potential measurements were performed on a Malvern Zetasizer Nano-S instrument, using clear disposable zeta cells.

TEM images were acquired on a Jeol 300 PX electron microscope. The gold nanoparticle diameters were measured automatically using the software ImageJ®.

TGA analysis was performed on a TGA Q5000 IR instrument.

UV-vis spectra were recorded on a Varian Cary50 Biospectrophotometer equipped with thermostatted multiple cell holders.

Fluorescence measurements were recorded on a Varian Cary Eclipse Fluorescence spectrophotometer equipped with a thermostatted cell holder.

2. Synthesis of ligand 1

Ligand **1** was synthetized, purified and characterized as described elsewhere.[1]

3. Synthesis and characterization of AuNP 1

AuNP **1** synthesized, purified and characterized as described elsewhere and stored in MilliQ water at 4 ºC.[1]

The size of the nanoparticles was assessed by TEM analysis as shown in Fig. S1.

Scale: 1 cm – 10 nm

Scale: 1 cm – 50 nm
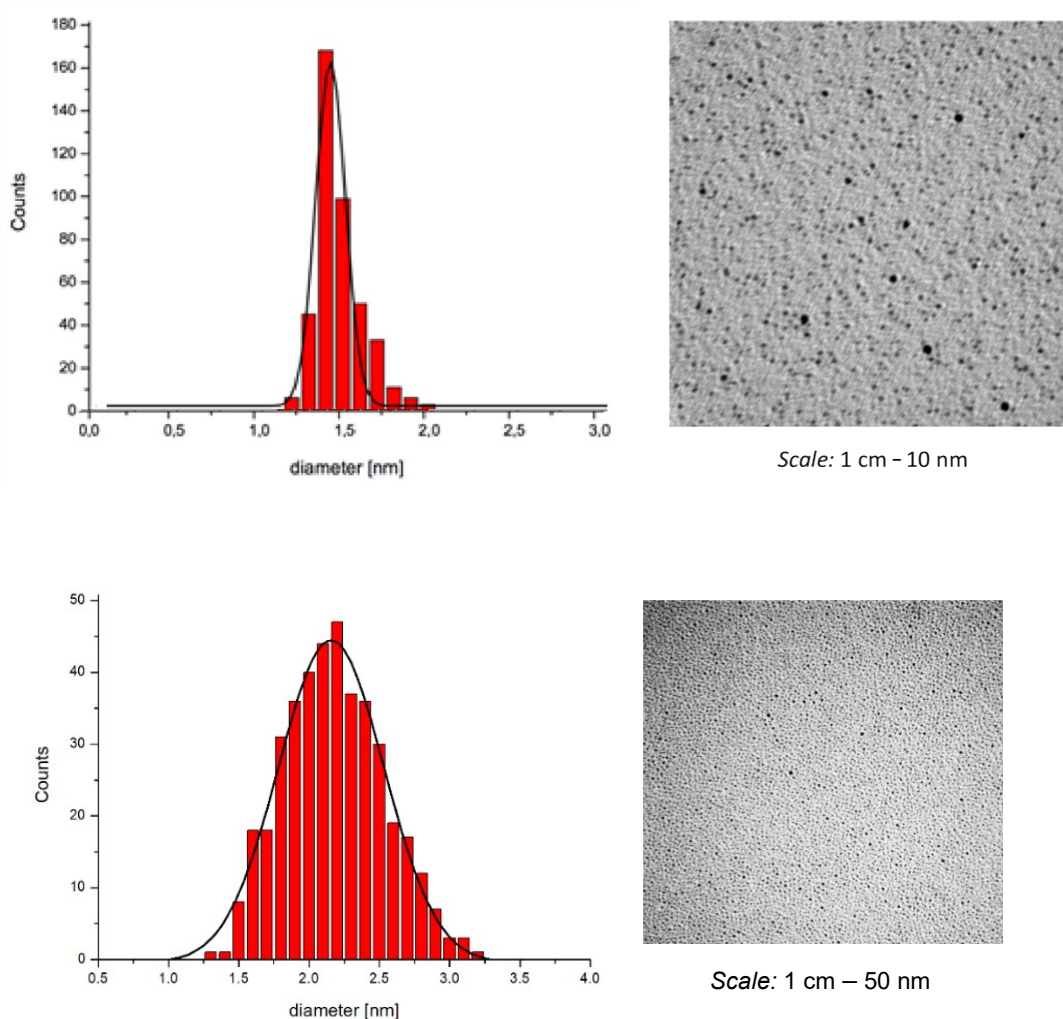
Figure S1. Top: TEM image and size distribution of AuNP **1** Average diameter = 1.5 nm (± 0.3 nm). Bottom: The same nanoparticles after the addition of **PIP3**. The average diameter grows to 2.2 nm (± 0.5 nm) and the size distribution is slightly larger.

4. Determination of the head group concentration of AuNP•1

The head group concentration of a solution of AuNP **1** was determined by monitoring the absorbance at 264 nm upon the addition of constant aliquots of $Cu(NO_3)_2$ as described by Scrimin *et al.* elsewhere.[2]

5. Displacement assays by fluorescence spectroscopy

5.1   Determination of the surface saturation concentration (SSC) of dATP$_{MANT}$

The surface saturation concentration of probe **dATP$_{MANT}$** ($\lambda_{ex/em}$ = 355/448 nm, slit 10/5 nm) on AuNP **1**•Zn^{II} was determined using fluorescence spectroscopy by titration in a buffered solution of AuNP **1**•Zn^{II} (10 μM, HEPES pH 7.0, 10 mM, 37 °C, Figure S1). New additions were only made after the

fluorescence signal had stabilized. The surface saturation concentration (SSC) was determined *via* extrapolation of the linear part of the titration curve, and represents the average of three independent repetitions. The SSC of **dATP_MANT** (3.3 ± 0.1 μM) is consistent with that reported in the literature.[3]
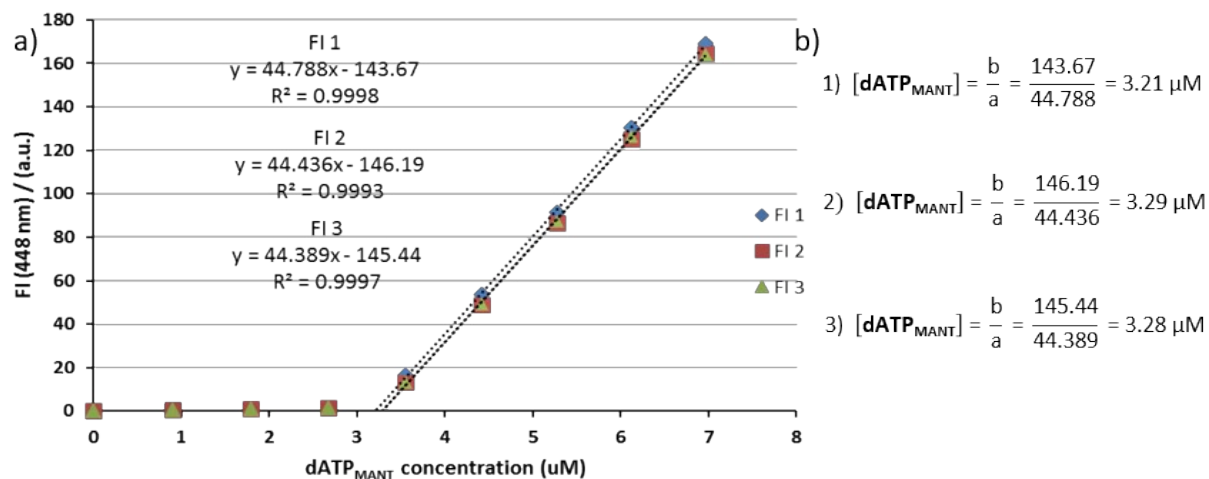
Figure S2   Titration experiments for the determination of the SSC of probe **dATP_MANT** on AuNP **1**·Zn^{II}. Conditions: [AuNP **1**·Zn^{II}] = 10 μM, [HEPES] = 10 mM, pH 7.0, 37 °C, $\lambda_{ex/em}$ = 355/448 nm, slit 10/5 nm.

5.2   Conversion curves from fluorescence intensity to concentration of displaced probes

Conversion curves fluorescence intensity → [displaced probe] were determined to compare displacement experiments performed at different slit values. A titration on a buffered solution (HEPES pH 7.0, 10 mM) of AuNP **1**·Zn^{II} (10 μM). The fluorescence intensity was measured in kinetic mode in order to ensure sample equilibration after each addition of fluorophore. By plotting the fluorescence intensity as a function of the concentration of fluorophore a linear increase was observed above the SSC of the fluorophore. Titrations were repeated three times and the concentration of displaced probe was normalized for the SSC of the fluorophore to obtain the percentage (Figure S2).

$$y = 187.3x - 568.83$$
$$R^2 = 0.9998$$

dATP$_{MANT}$, slit 10/10 nm:

$$[\textbf{dATP}_{MANT}\ \text{displaced}]=\frac{FI+568.83}{187.3}-3.04$$

$$\%\ \textbf{dATP}_{MANT}\ \text{displaced}=\frac{[\textbf{dATP}_{MANT}\ \text{displaced}]}{3.26}\times100$$
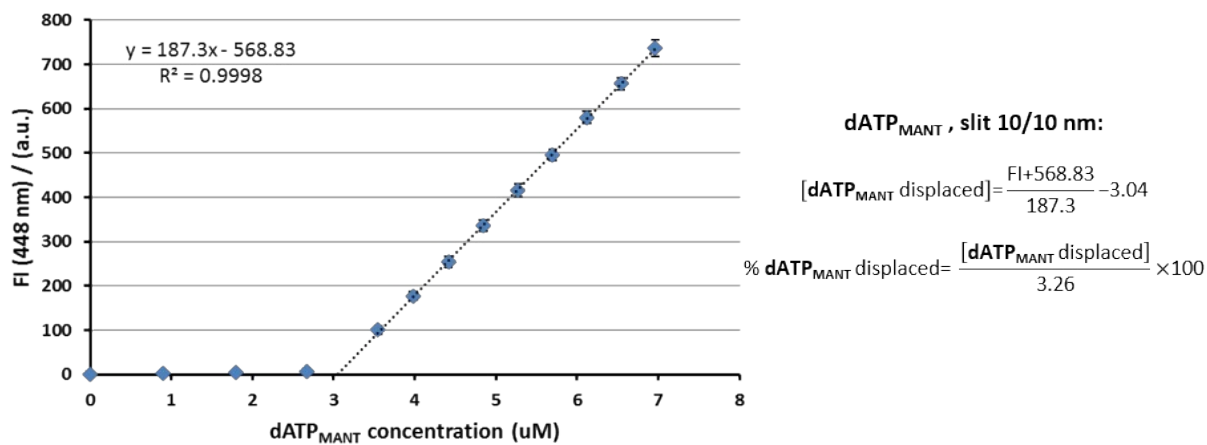
Figure S3 Conversion curved FI / [displaced **dATP$_{MANT}$**] for b) **dATP$_{MANT}$** using ex/em slit of 10/5 nm and c) **dATP$_{MANT}$** using ex/em slit of 10/10 nm. Experimental conditions: [AuNP **1**·Zn^{II}] = 10 μM, [HEPES] = 10 mM, pH 7.0, 37 °C, $\lambda_{ex/em}$ = 355/448 nm.
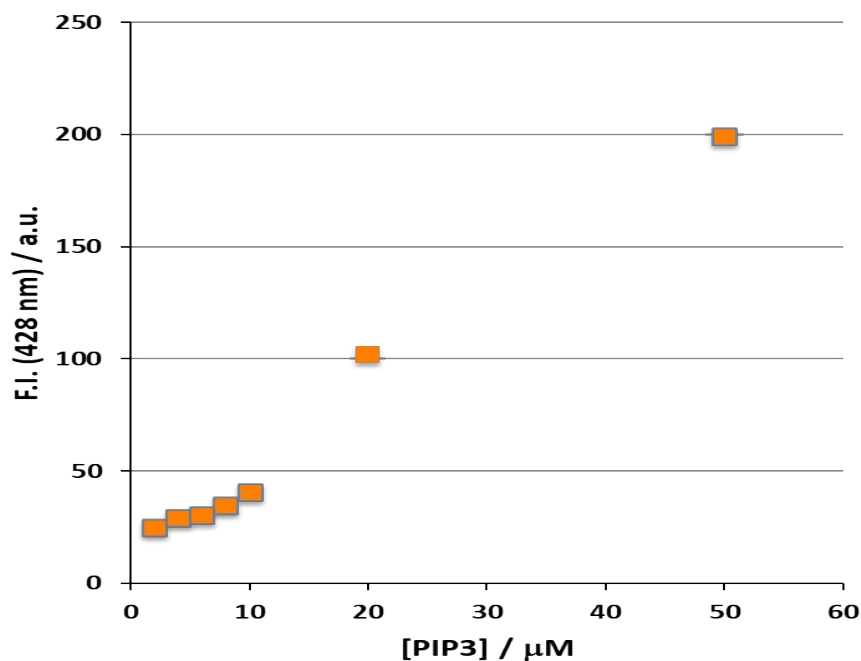
Figure S4 Determination of the cac of **PIP3** by fluorescence spectroscopy. The FI values are plotted as function of the phosphoinositide concentration. Experimental conditions: [**DPH**] = 2 μM, [HEPES] = 10 mM, pH 7.0, $\lambda_{ex/em}$ = 355/428 nm, slit 5/10 nm, 37 °C.

5.3   Determination of the critical aggregation concentration (cac) of phosphoinositides

The critical aggregation concentration (cac) of PIP3 was determined by using 1,6-diphenyl-1,3,5-hexatriene (**DPH**) as the fluorescent probe. **DPH** is not soluble in water and it does not give a fluorescent signal. The FI increases only in the presence of apolar aggregates, in which **DPH** is solubilized. The concentration at which PIP3 begins to aggregate was determined by extrapolation of the linear part of the titration curve. **PIP3** does have a cac of ca. 10.5 μM, confirming the values reported in the literature.[4–6]

5.4   Displacement experiments by fluorescence spectroscopy

All displacement experiments were performed by titration one of the phosphoinositides of interest in a buffered solution (10 mM HEPES, pH 7.0) of AuNP **1**•Zn^{II} (10 μM) and probe **dATP$_{MANT}$** at 100% of its SSC (3.3 μM). Consecutive additions of the phosphoinositide of interest (using a 0.1 mM solution for additions in the 0.1–1 μM range, and a 1 mM one for additions >1 μM) were only made after the fluorescence signal had stabilized (especially for PIP3). The FI values were then converted in % of displaced probe using the conversion curve showed above (Figure S4). Data are reported as averaged values from three independent repetitions.
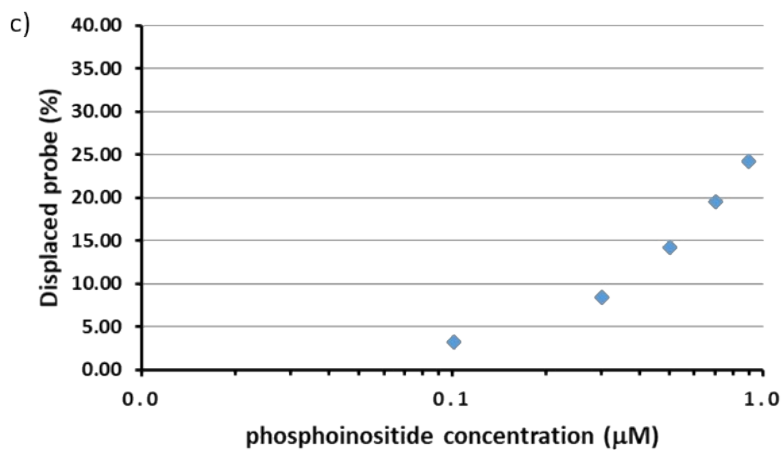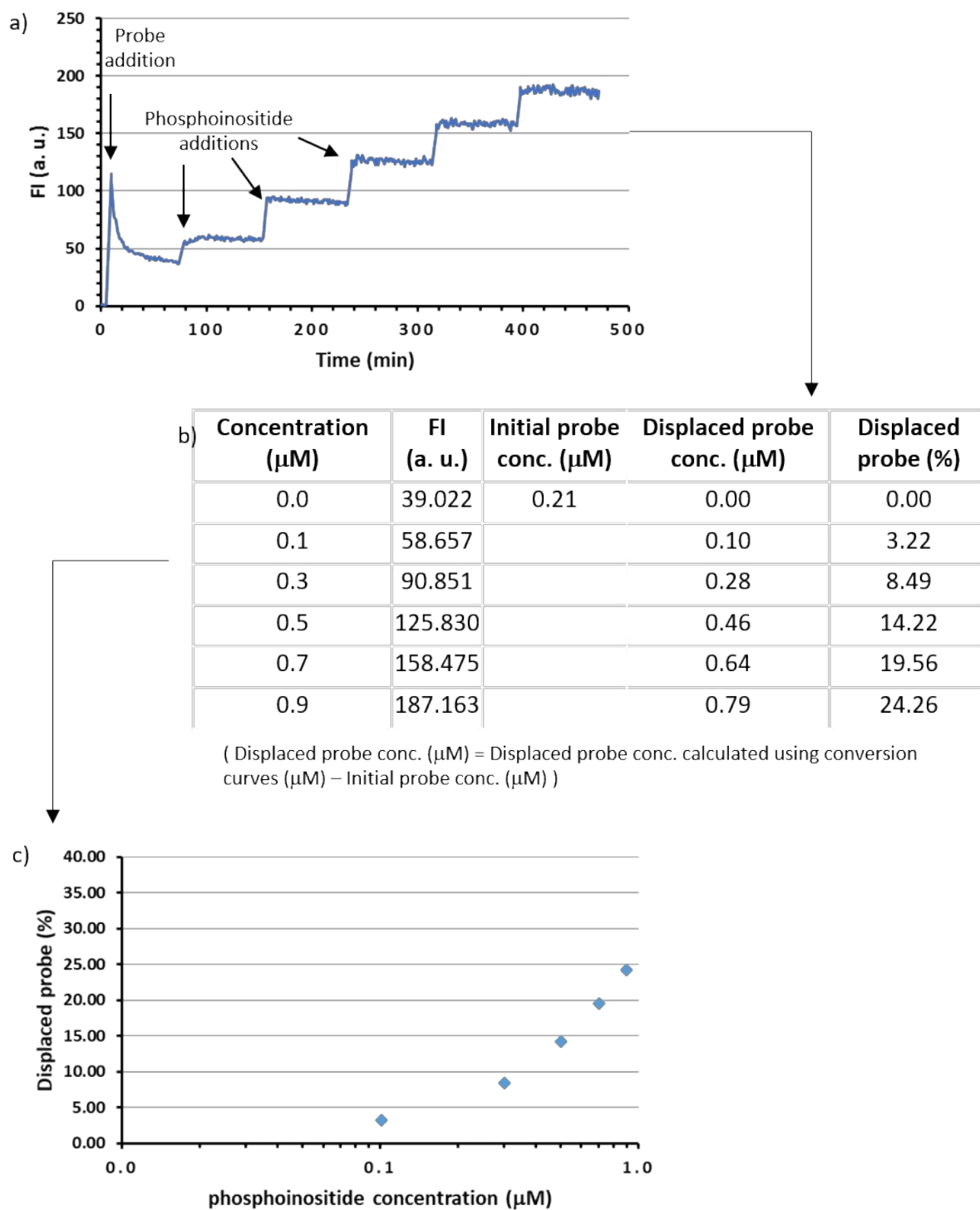
Figure S5   Representative example of displacement assay by fluorescence spectroscopy. a): FI recorded in kinetic mode. b): calculation of % of displaced probe from the averaged FI values and normalization to the initial concentration of unbound probe. c): % of displaced probe as a function of [phosphoinositide].

6.   Detection of PIP3 in simulated lung fluids (SLFs) with AuNP 1•Zn^{II}

Three solutions were used to simulate pulmonary fluids: SLF1, SLF3 and SLF4, that are three of the five most used simulated lung fluids (SLFs).[7] SLFs composition is listed in Table S1. SLF1 is the artificial lysosomal fluid (ALF), which represents the fluid with which inhaled particles come into contact during the phagocytosis process by alveolar and interstitial macrophages. SLF1 has a pH of 4.5, similar to the phagolysosomal pH of macrophages.[7,8] SLF3 and SLF4 simulate the interstitial (extracellular) fluid: in particular, SLF4 is identical to SLF3 with the addition of dipalmitoylphosphatidylcholine (DPPC). DPPC simulates the lung surfactant, constantly produced by the epithelial cells, which consists of lipid-rich lipoproteins with a lipid content dominated by phosphatidylcholine with a high content of palmitic acid. Both SLF3 and SLF4 have a pH of 7.4.[7]

Table S1   Composition of simulated lung fluids SLF1, SLF3 and SLF4.

	SLF1 / mM	SLF3 / mM	SLF4 / mM
$MgCl_2$	0.53	–	–
$MgCl_2 \cdot 6H_2O$	–	1.00	1.00
NaCl	54.93	103.00	103.00
KCl	–	4.00	4.00
Na_2HPO_4	0.50		
Na_2SO_4	0.27	0.50	0.50
$CaCl_2 \cdot 2H_2O$	0.87	2.50	2.50
Sodium acetate trihydrate	–	7.00	7.00
$NaHCO_3$	–	31.00	31.00
Sodium citrate dihydrate	0.26	0.33	0.33
NaOH	150	–	–
Citric acid	108.27	–	–
Glycine	0.79		
Sodium lactate	0.76		
Sodium pyruvate	0.78		
NaH_2PO_4	–	1.03	1.03
Dipalmitoyl phosphatidyl choline (DPPC)	–	–	0.27

6.1   Determination of the SSC of probe A in SLF1, SLF3 and SLF4

SLF1, SLF3 and SLF4 were used as received.
The SSC values of probe **dATP$_{MANT}$** in SLFs were determined by fluorescence spectroscopy as described in Section 5.1 (Figure S5).
$SSC_{(SLF1)} = 0.9 \pm 0.1 \ \mu M$
$SSC_{(SLF3)} = 1.1 \pm 0.2 \ \mu M$
$SSC_{(SLF4)} = 1.0 \pm 0.1 \ \mu M$

a)

FI 1
y = 36.618x - 34.214
R² = 0.9972

FI 2
y = 37.662x - 28.811
R² = 0.9992

FI 3
y = 36.603x - 31.979
R² = 0.9981

d)

1) $[\mathbf{dATP_{MANT}}] = \dfrac{b}{a} = \dfrac{34.214}{36.618} = 0.93 \ \mu M$

2) $[\mathbf{dATP_{MANT}}] = \dfrac{b}{a} = \dfrac{28.811}{37.662} = 0.76 \ \mu M$

3) $[\mathbf{dATP_{MANT}}] = \dfrac{b}{a} = \dfrac{31.979}{36.603} = 0.87 \ \mu M$

b)

FI 1
y = 46.504x - 59.7
R² = 0.9985

FI 2
y = 48.557x - 47.385
R² = 0.9991

FI 3
y = 47.502x - 47.01
R² = 0.9997

e)

1) $[\mathbf{dATP_{MANT}}] = \dfrac{b}{a} = \dfrac{59.7}{46.504} = 1.28 \ \mu M$

2) $[\mathbf{dATP_{MANT}}] = \dfrac{b}{a} = \dfrac{47.385}{48.577} = 0.98 \ \mu M$

3) $[\mathbf{dATP_{MANT}}] = \dfrac{b}{a} = \dfrac{47.01}{47.502} = 0.99 \ \mu M$

c)

FI 1
y = 44.091x - 42.233
R² = 0.9998

FI 2
y = 44.673x - 44.338
R² = 0.9999

FI 3
y = 44.26x - 44.285
R² = 0.9999

f)

1) $[\mathbf{dATP_{MANT}}] = \dfrac{b}{a} = \dfrac{42.233}{44.091} = 0.96 \ \mu M$

2) $[\mathbf{dATP_{MANT}}] = \dfrac{b}{a} = \dfrac{44.338}{44.673} = 0.99 \ \mu M$

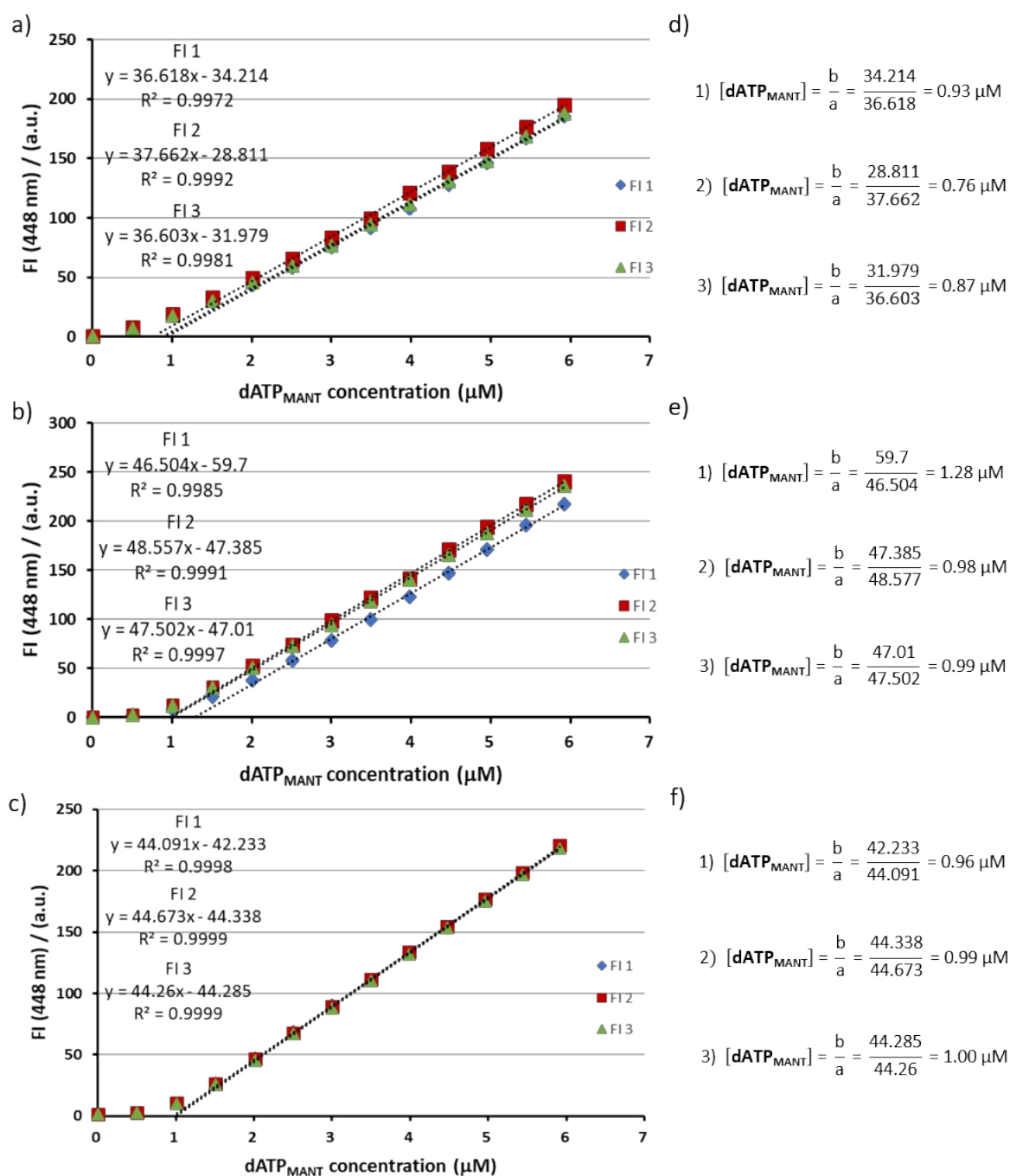3) $[\mathbf{dATP_{MANT}}] = \dfrac{b}{a} = \dfrac{44.285}{44.26} = 1.00 \ \mu M$

Figure S6 Determination of the SSC of probe **dATP_MANT** on AuNP **1**•Zn^{II} in simulated lung fluids (SLFs). Experimental conditions: [AuNP **1**•Zn^{II}] = 10 μM, $\lambda_{ex/em}$ = 355/448 nm, slit 10/5 nm, 37 °C. a-c): FI values plotted as a function of [**A**] and determination of the SSC *via* extrapolation of the curves in fluids SLF1 (a), SLF3 (b) and SLF4 (c). d-f): calculaton of the SSC values in fluids SLF1 (d), SLF3 (e) and SLF4 (f).

6.2 Conversion curves from fluorescence intensity to concentration of displaced probes in SLFs media

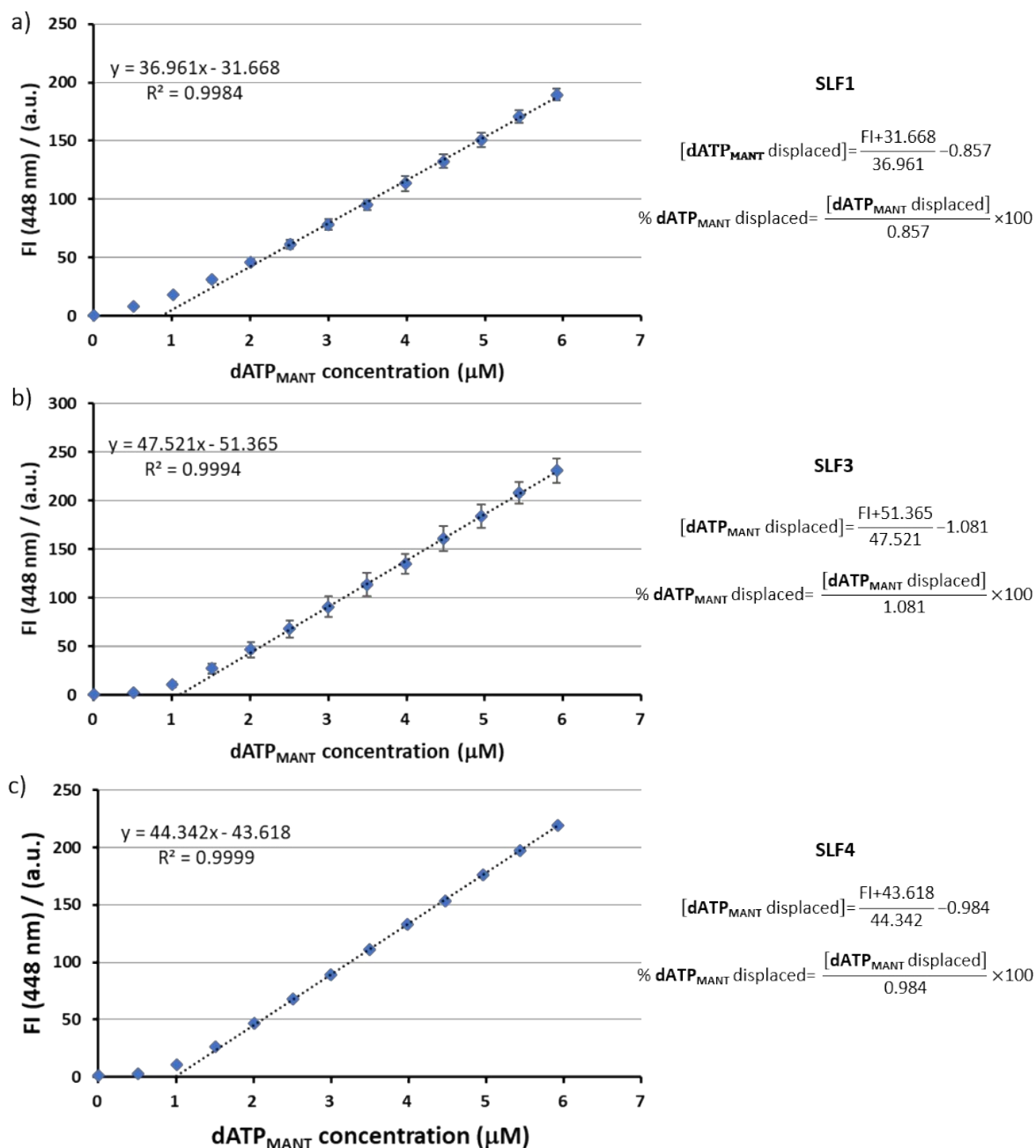Conversion curves fluorescence intensity → [displaced probe] were determined as described in Section 5.2 .

a) SLF1

$$y = 36.961x - 31.668$$
$$R^2 = 0.9984$$

$$[dATP_{MANT} \text{ displaced}] = \frac{FI + 31.668}{36.961} - 0.857$$

$$\% \, dATP_{MANT} \text{ displaced} = \frac{[dATP_{MANT} \text{ displaced}]}{0.857} \times 100$$

b) SLF3

$$y = 47.521x - 51.365$$
$$R^2 = 0.9994$$

$$[dATP_{MANT} \text{ displaced}] = \frac{FI + 51.365}{47.521} - 1.081$$

$$\% \, dATP_{MANT} \text{ displaced} = \frac{[dATP_{MANT} \text{ displaced}]}{1.081} \times 100$$

c) SLF4

$$y = 44.342x - 43.618$$
$$R^2 = 0.9999$$

$$[dATP_{MANT} \text{ displaced}] = \frac{FI + 43.618}{44.342} - 0.984$$

$$\% \, dATP_{MANT} \text{ displaced} = \frac{[dATP_{MANT} \text{ displaced}]}{0.984} \times 100$$

Figure S7   Conversion curves FI → [displaced probe] and calculation of the percentage of displaced probe dATP_MANT in fluid SLF1 (a), SLF3 (b) and SLF4 (c). Experimental conditions: [AuNP **1**•Zn^{II}] = 10 µM, $\lambda_{ex/em}$ = 355/448 nm, slit 10/5 nm, 37 ºC.

6.3 Displacement experiments in SLFs by fluorescence spectroscopy

All displacement experiments in SLFs and the kinetic studies were performed following the same procedure described in Section 5.4. **PIP3** was titrated in a solution of AuNP **1**•Zn^{II} (10 μM) and probe **d**ATP$_{MANT}$ (100% SSC). Samples were prepared by adding to the simulated fluid firstly AuNP **1**•Zn^{II}. The mixture was incubated for 5 minutes at 37 ºC followed by addition of probe **d**ATP$_{MANT}$. No buffer was used.

7. Zeta-potential analysis

Samples for zeta potential measurements were prepared by adding to a 10 μM buffered solution of AuNP **1**•Zn^{II} ([HEPES, pH 7.0] = 10 mM, total volume = 1 mL) different amounts of phosphoinositide. In particular, 16 samples were prepared for each phosphoinositide, at 0.05, 0.1, 0.25, 0.5, 0.75, 1, 1.2, 1.4, 1.6, 1.8, 2, 2.5, 3, 4, 6 and 8 μM, and a sample with AuNP **1**•Zn^{II} 10 μM only. Samples were prepared at least 24 h before the analysis to allow sample equilibration.

For the kinetic studies, samples were prepared immediately before the analysis, setting a delay of 300 s between each measurement. The evolution of the ζ-potential (Figure S8) of a buffered solution of AuNP **1**•Zn^{II} (10 μM) in the presence of **IP3** or **PIP3** (10 μM) was recorded over time. **IP3** requires several hours to achieve zeta potential stabilization. On the other hand, **PIP3** achieves signal stabilization within 1 h.

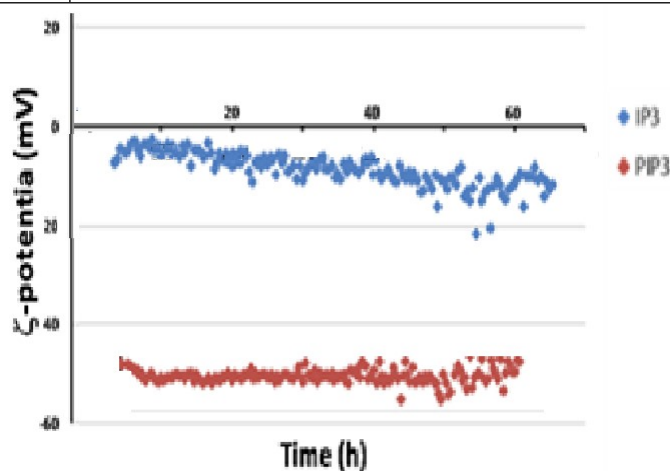| MATERIAL	Au (RI = 0.197, absorption = 0.400)
DISPERSANT	Water (T = 25 ºC, η = 0.8872 cP, RI = 1.330, ε = 78.5)
MODEL	Smoluchowsky
TEMPERATURE	25 ºC (equilibration time = 30 s)
CELL	DTS1060C
MEASUREMENT	Duration: automatic (min runs = 10, max runs = 100, No runs = 3, Delay = 0 s)

Figure S8. Zeta Potential evolution over time in the presence of **IP3** (blue) and **PIP3** (red). Experimental conditions: [AuNP **1**•Zn^{II}] = 10 μM, [HEPES, pH 7.0] = 10 mM, 25 ºC.

8. Concentration of PIP3 and extraction with AuNP 1•Zn^{II}

8.1 Optimization of the conditions for complete precipitation of AuNP 1•Zn^{II} with diethyl ether

Samples for the precipitation with diethyl ether were prepared by adding AuNP **1**•Zn^{II} (10 μM) to a buffered solution ([HEPES pH 7.0, 10 mM; total volume: 1 mL. Then, 400 μL of diethyl ether were added. The sample was then vortexed for 5 min and centrifuged for 40 min at 14000 rpm. After centrigugation, >90% of NPs had precipitated from the solution.
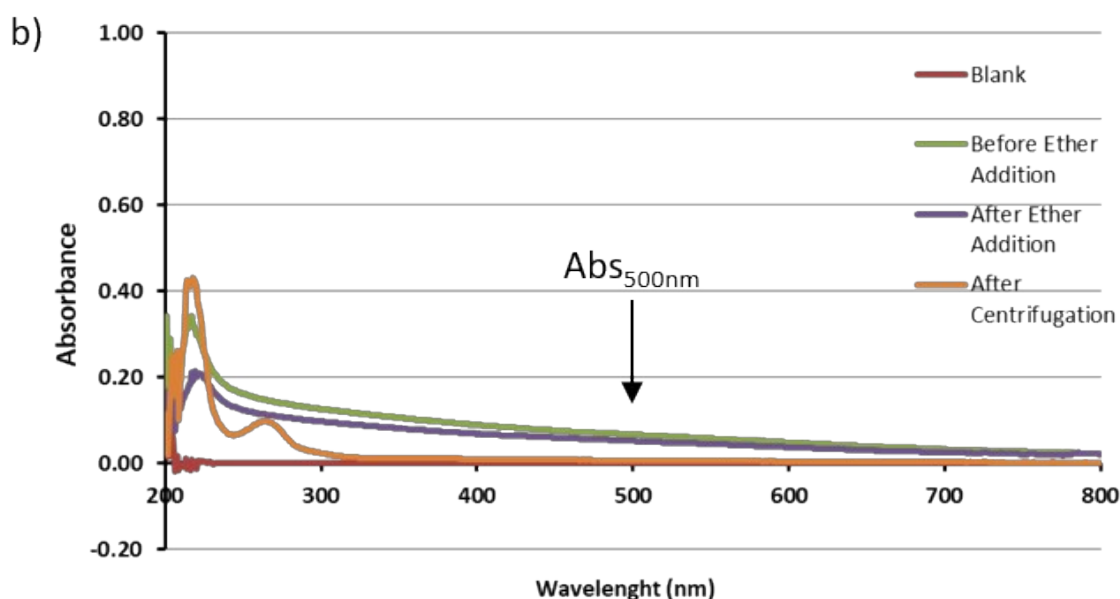

Figure S9   Normalized UV/Vis spectra of a solution of AuNP **1**•Zn^{II} (10 μM, [HEPES] = 10 mM, pH 7.0, 25 °C) before diethyl ether addition (green), after ether addition (violet) and after precipitation *via* centrifugation (orange). Experimental conditions: [HEPES, pH 7.0] = 10 mM, 25 ºC.

9. Determination of dissociation constants of the compounds reported in Table 1 (main text)

Dissociation constants for DMP,[9] HPNP,[9] and UPNP[10] were reported in the quoted references and obtained from Michaelis-Menten treatment of the kinetic data.

The dissociation constants for cAMP, AMP, ADP, and ATP were obtained from the IC$_{50}$ values reported in the literature[11] acquired from inhibition of the hydrolysis of HPNP by the different anions. The following equation was used:

(1) $K_d = (IC_{50} \times K_{d,HPNP})/(K_{d,HPNP} + [HPNP])$

The dissociation constant of $dATP_{MANT}$ was determined by interpolation of the binding isotherm reported[12] for ATP in the presence of a fixed amount of $dATP_{MANT}$ as a competitor using the following equation:[13]

(2) $K_{d,ATPapp} = K_{d,ATP} \times (1 + [dATP_{MANT}]/K_{d,dATPMANT})$

Because of the conditions of the experiment the value of $K_{d,dATPMANT}$ is likely underestimated.

10. References

[1]   G. Pieters, A. Cazzolaro, R. Bonomi, L. J. Prins, *Chem. Commun.* **2012**, *48*, 1916–1918.

[2]   G. Zaupa, C. Mora, R. Bonomi, L. J. Prins, P. Scrimin, *Chem. Eur. J.* **2011**, *17*, 4879–4889.

[3]   G. Pieters, C. Pezzato, L. J. Prins, *Langmuir* **2013**, *29*, 7180–7185.

[4]   F. L. Huangs, K.-P. Huang, *J. Biol. Chem.* **1991**, *266*, 8727–8733.

[5]   R. B. Campbell, F. Liu, A. H. Ross, *J. Biol. Chem.* **2003**, *278*, 33617–33620.

[6]   W. Huang, D. Jiang, X. Wang, K. Wang, C. E. Sims, N. L. Allbritton, Q. Zhang, *Anal. Bioanal. Chem.* **2011**, *401*, 1881–1888.

[7]   M. R. C. Marques, R. Loebenberg, M. Almukainzi, *Dissolution Technol.* **2011**, *18*, 15–28.

[8]   W. Stopford, J. Turner, D. Cappellini, T. Brock, *J. Environ. Monit.* **2003**, *5*, 675–680.

[9]   J. Czescik, S. Zamolo, T. Darbre, F. Mancin, P. Scrimin, *Molecules*, **2019**, *24*, 2814.

[10]   J. Czescik, F. Mancin, R. Strömberg, P. Scrimin, *Chem European J*, **2021**, *27*, 8143–8148.

[11]   R. Bonomi, A. Cazzolaro, A. Sansone, P. Scrimin, L. J. Prins, *Angewandte Chemie (International ed. in English)*, **2011**, *50*, 2307–2312.

[12]   G. Pieters, C. Pezzato, L. J. Prins, *Langmuir*, **2013**, *29*, 7180−7185.

[13]   E. C. Hulme, M. A. Trevethick, *Brit J Pharmacol*, **2010**, *161*, 1219–1237.